ROYAL SOCIETY OF CHEMISTRY

PAPER

Check for updates

Harnessing de-oiled *Glycine max* seed-anchored-CuO nanoparticles for adsorptive removal of crystal violet dye with comprehensive mechanistic insights

Mahnoor Usman,[a] Fozia Batool, [ID] *[a] Tunzeel Iqbal,[b] Sobia Noreen,[a] Humaira Yasmeen Gondal,[a] Taleeha Roheen,[a] Rahman Qadir,[c] Muhammad Amin,[d] Sayyam Sajid[a] and Allah Ditta [ID] *[e]

A novel solution is introduced by harnessing the power of de-oiled *Glycine max* L. seeds (DO/S) and enhancing them with copper oxide-loaded nanoparticles (DO/S NPs) to effectively eradicate the toxic dye crystal violet (triarylmethane dye) from aqueous solutions. The presence of peaks at 653.87 cm^{-1} and 567.07 cm^{-1} in FTIR spectra confirmed the presence of CuO NP loading on *G. max* L. seeds. Furthermore, the smooth spherical cavities facilitated crystal violet adsorption, as revealed by SEM analysis. PZC results revealed that adsorption is more efficient under neutral and basic conditions (pH 7, 9, and 11) for DO/S, whereas DO/S NPs as an adsorbent facilitate excellent crystal violet removal in basic media (pH 9 and 11). Thermogravimetric analysis showed that major weight loss occurs at 21.49 min, 446 °C (DO/S), and at 22.64 min, 467.47 °C (DO/S NPs). Thermodynamics studies revealed less randomness, spontaneity, and favorable adsorption reactions by the copper-loaded adsorbent. Kinetics studies showed that the employment of a pseudo-second-order kinetic model efficiently fitted the obtained experimental data ($R^2 \geq 0.99$). A batch experiment was performed by applying varying adsorption parameters. In comparison to DO/S, DO/S NPs exhibited an improved maximum removal rate, *i.e.* a rate of 95% at a dye concentration of 80 ppm, a contact time of 90 minutes, 293.15 K, pH 9, and an adsorbent dose of 1 g. Since de-oiled *G. max* L. is an industrial byproduct, its potential as an adsorbent for textile dye removal is an effective approach toward a clean environment for future generations.

Introduction

One of the noteworthy challenges of today's world is to eradicate the hazardous impacts of pollutants and prevent the degradation of natural resources. Globalization has left an imprint of instability on the earth, especially regarding water pollution. Harmful pollutants do not just affect water bodies but can also have an impact on various human activities such as public health. Water contamination can be due to physical, chemical, or biological pollutants.[1]

Escalating industrialization has jeopardized terrestrial and aquatic biota through the most common pollutant, *i.e.*, dyes. The textile industry releases 10% of its annual dye production

(700 000 tons) as waste. Many industries, such as the paper, tanning, pharmaceutical, and cosmetic industries, consume over 10 000 dyes.[2] Owing to molecular solid formation, dyes act as carcinogenic or mutagenic agents.[3]

In recent decades, pharmaceuticals have also contributed to environmental contaminants that resist traditional treatment methods. Studies have shown that there is an urgent need for innovative, efficient treatment strategies to safeguard water resources and public health.[4] Similarly, the removal of high concentrations of heavy metals, such as Ni^{2+} and Co^{2+}, from electroplating wastewater is another challenge. Recent studies have highlighted the surface functionalization of materials such as layered double hydroxides (LDHs) as an effective approach for enhancing adsorption capacities and improving the efficiency of wastewater remediation.[5] Wastewater treatment has attracted much research interest as pollutant dyes in water bodies do not allow sunlight penetration and ceases the photosynthetic activity in water bodies. Dyes pollution may also pose skin irritation problems, mutation in humans, or skin allergies in humans. Cationic dyes are widely used as a coloring or staining agent in the pharmaceutical, cosmetic, and textile

[a]Institute of Chemistry, University of Sargodha, Sargodha 40100, Pakistan. E-mail: fozia.batool@uos.edu.pk

[b]Department of Chemistry, Rawalpindi Women University, Rawalpindi, Pakistan

[c]Department of Food Technology, Faculty of Food Science and Technology, Universiti Putra Malaysia, Serdang, Selangor, 43400, Malaysia

[d]Department of Chemistry, University of Lahore, Sargodha Campus, Pakistan

[e]Department of Environmental Sciences, Shaheed Benazir Bhutto University Sheringal, Dir (Upper), 18000, Pakistan. E-mail: allah.ditta@sbbu.edu.pk

industries.[6] Thus, the increased utilization of these dyes has led to an increase in water pollution.

The cationic crystal violet is extremely toxic due to its carcinogenic nature, even at 1 milligram per liter.[7] Scientific research has explored various methods for dye removal, including flocculation, coagulation, ion exchange method, adsorption on active carbon and oxidation.[8] Out of all these methods, the adsorption method is the optimal choice because of its cost-effective and eco-friendly properties.[9] These methodologies come with certain protocols, such as the requirement of qualified staff, processing machines, and a wide variety of chemicals. Thus, they seem incompatible for decontamination purposes compared to the adsorption method. Therefore, the adsorption method is the prime choice due to its versatility and cost-effectiveness. The adsorbent materials help hold and remove the dye particles. Moreover, these adsorbents are not limited to one dye, but are usable for a wide range of industrial dye effluents. The regeneration and reuse of many adsorbents have targeted economic viability.[10] Furthermore, the easy integration of adsorption into other technologies makes it more beneficial. In conclusion, an eco-friendly, sustainable water treatment and economically viable method is present in adsorption.

In this context, agro-waste is an effective adsorbent that elevates and enhances the dye-removal process. *Glycine max* L. (commonly known as the soybean), a member of the Leguminosae family, is considered a nutritional and medicinal ingredient.[11] Isoflavonoids, flavonoids, phenolics, tannins, proanthocyanidins, and phenolics are the key constitutional functional groups of *Glycine max* L. 70% of the world's soy production comes from China, Brazil, and the U.S. Moreover, extracted soy oil and protein are processed food ingredients.[12] Therefore, the de-oiled soybean seeds play a role as an effective, eco-friendly adsorbent for the decontamination of crystal violet dye.

Conventional adsorbents such as activated carbon, natural clay, zeolites, limestone, agro, and industrial waste have become barriers to decontamination.[13] The significant limitations of conventional adsorbents include their complex, multi-step synthesis process, removal of garbage at ppb levels, and separation from the treated water.[14] Therefore, nanoparticles have revolutionized water treatment by overcoming these hurdles. Research has shown that nanoparticles, having a high surface area and reactive sites, are efficient in dye removal. Moreover, the coat's effectiveness and ease of disposal pave the way for its feasibility in environmental application. CuO-NPs have been primarily used for dye removal due to their unique adsorption properties, which include many active sites and affordability.[15]

The absorptive potential of de-oiled soybean and the nanoparticles comprise the excellent adsorbent. The copper oxide CuO-NPs are loaded onto the surface of de-oiled soya beans to form a superb sorbent. Copper nanoparticles were prepared and loaded on the surface of DO/S to enhance its absorptive power. This sorbent is a cost-effective and sustainable approach for removing cationic crystal violet. Thus, comparing the adsorption potential of DO/S and the DO/S-NPs seems clear. Furthermore, adsorption parameters such as concentration, time,

amount of adsorbent, temperature, and pH were varied to optimize this study. The DO/S showed the maximum adsorption of 90% with 1 g of adsorbent. Meanwhile, the DO/S-NPs showed a 95% maximum removal of crystal violet dye with 1 g of adsorbent dose. Adsorption kinetics and isotherms were also performed to more accurately evaluate the results.

This revolutionary approach to water treatment has been developed with the creation of a groundbreaking modified adsorbent, setting a new benchmark in eco-friendly innovation. Using precisely optimized DO/S-NPs, this method has successfully targeted and removed the cationic crystal violet with unparalleled efficiency. The effectiveness of this study is further validated by comparative analysis and robust experimental results, solidifying its position as a game-changing breakthrough in enhancing sustainable environmental remediation. In summary, the de-oiled soybean seeds loaded with copper nanoparticles have amplified the potential decontamination of water from hazardous dyes. Moreover, this method finds application on an industrial scale due to its wide accessibility and cost-efficiency.

Material and methods

Material and equipment

All the materials, chemicals, and apparatus used in this research were of analytical grade with high quality and purity. The chemicals that were used in this study included copper(II) nitrate trihydrate ($Cu(NO_3)_2 \cdot 3H_2O$), citric acid ($C_6H_8O_7$), (NaOH) with 98% purity, and conc. HCl. The distilled water used in this study was from the Khushab plant at the University of Sargodha. DO/S and DO/S NPs were synthesized from the *Glycine max* L. seeds. *Glycine max* L. seeds were obtained from Sargodha.

Preparation of de-oiled *Glycine max* L. (DO/S)

Glycine max L. was washed 5–6 times with distilled water to remove dust and impurities. After drying in an open space, they passed through mild grinding using a mortar and a pestle. Then, the ground seeds were soaked in *n*-hexane and heated at 75 °C. After half an hour of heating, the seeds were protected with aluminum foil and left for 2 hours. A top yellow oily layer can be observed in a beaker. The dried *Glycine max* L. seeds were washed with distilled water 6–7 times to remove the *n*-hexane. The obtained seeds were then dried in the sun for three days. The dried seeds were ground into a fine powder and passed through sieves to obtain finely divided de-oiled *Glycine max* L.

Synthesis of de-oiled *Glycine max* L. loaded with CuNPs (DO/S NPs)

To synthesize DO/S NPs, copper(II) nitrate trihydrate was used as the precursor salt and citric acid as the reducing agent. In the first step, 1 mM (0.192 g in 1000 mL) citric acid solution was prepared in distilled water. The pH of the citric acid solution was approximately 6.5 to 7. DO/S (6 g) was added to the citric acid solution with vigorous stirring for 2 hours. In the second step, DO/S were filtered and oven-dried at 70 °C for 3 hours. The
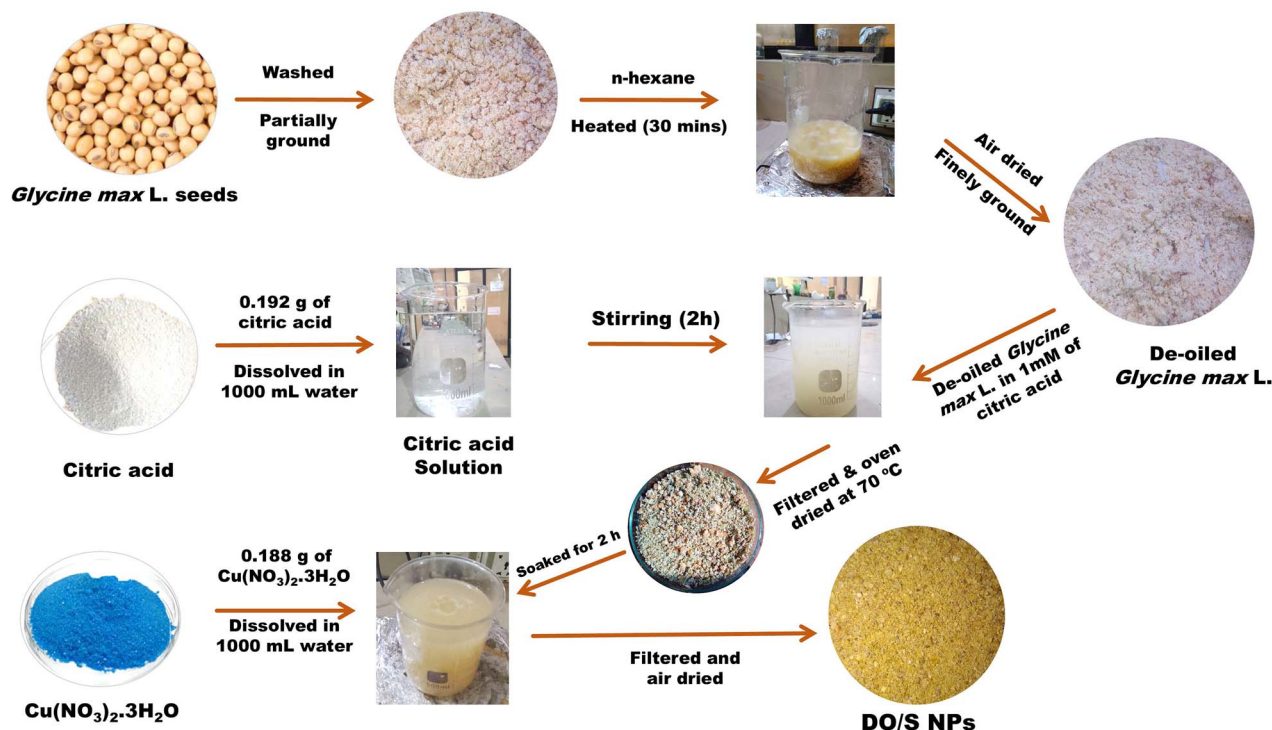
Fig. 1 Synthesis of de-oiled *Glycine max* L. loaded with copper nanoparticles (DO/S NPs).

seeds were taken out of the oven once they completely dried. In the third step, 1 mM (0.188 g in 1000 mL) of copper(II) nitrate trihydrate solution was prepared in distilled water. The pH of this solution was approximately 6.5, which helped facilitate the formation of CuO nanoparticles. The dried DO/S were soaked in a salt solution for 2 hours. The treatment was then followed by filtration and air drying. The resulting product is freshly prepared de-oiled *Glycine max* L. loaded with CuO nanoparticles (Fig. 1). The theoretical yield of CuO nanoparticles was calculated based on the following stoichiometric equation:

$$2Cu(NO_3)_2 \cdot 3H_2O + C_6H_8O_7 \rightarrow 2CuO + 4NO_2 + 3H_2O + 6CO_2$$
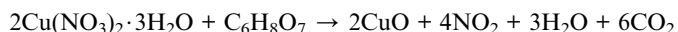
Crystal violet was selected as a sorbent to evaluate the adsorption capability of DO/S and DO/S Cu NPs. The theoretical yield is based on 7.53×10^{-4} mol of $Cu(NO_3)_2 \cdot 3H_2O$ used, which would produce 0.060 g of CuO. The actual yield of CuO nanoparticles was measured as 0.050 g, and the reaction yield of DO/S NPs was calculated at approximately 83.3% using the following formula:

$$\text{Reaction yield}(\%) = \frac{\text{actual yield}}{\text{theoretical yield}} \times 100$$

These adsorbents, *i.e.*, DO/S and DO/S NPs, were stored in airtight bottles or bags to avoid any contamination.

Characterization of the DO/S NPs

The synthesized adsorbents (DO/S and DO/S NPs) were analyzed *via* energy-dispersive X-ray (EDX), scanning electron microscopy (SEM), ultraviolet-visible spectrometer, and Fourier transform infrared spectroscopy (FT-IR). The structural characteristics and chemical formulation of the DO/S NPs were analyzed and evaluated by SEM-EDX. The samples were sheathed with a small layer of gold to generate electrical conductivity on the powdery surface of the DO/S NPs before being calcined at 250 °C. FTIR (Nicolet 6700, the mode Fisher, Waltham, MA, USA) was used to analyze the chemical bonding in the synthesized materials. With a resolution of 4 cm^{-1}, the range covered by this instrument was 4000–400 cm^{-1}. Brunauer–Emmett–Teller (BET) analysis was performed using a surface area analyzer (NOVA 2200e Quanta Chrome, USA) for surface characterization of the sample using N$_2$ as a standard.

TGA analysis

TGA of de-oiled *Glycine max* L. (DO/S) and de-oiled *Glycine max* L. loaded with CuO nanoparticles (DO/S NPs) was carried out by employing an SDT650 thermal analyzer. A sample weighing 8.188 mg for DO/S and 7.703 mg for DO/S NPs was exposed to heating at 20 °C min^{-1} with a nitrogen flow (10 mL min^{-1}) within the temperature range of 20 to 467.47 °C. The thermal treatment began at approximately room temperature, with a gradual elevation of the temperature leading to weight loss due to volatile content. As the temperature increased, significant weight loss occurred, which was associated with the pyrolysis of *Glycine max* L. and the decomposition of CuO nanoparticles.

Determination of the point of zero charge (PZC)

The salt addition method was used to evaluate the point of zero charge of the DO/S and DO/S NPs. In this method, 500 mL of 0.1 M of sodium nitrate solution was prepared in the flask. From this solution, 50 mL was taken out and transferred to 10

different conical flasks. The pH (3–11) was adjusted in each flask with 0.1 M HCl and 0.1 M NaOH. After adjusting the pH, 1 g DO/S was added to five flasks, and DO/S NPs were introduced to the other five flasks containing the solution of varying pH levels. Then, these solutions were ready to go through the 24 hours of agitation in the orbital shaker. After completion of the reaction, the solutions were filtered and the change in pH was carefully checked with a pH meter.[16,17]

The following equation was used to compute the altered pH, where pH_o is the initial pH before agitation, and pH is the final pH after agitation:

$$\Delta pH = pH_o - pH$$

The ΔpH values were plotted against the initial pH values to evaluate the PZC. The point coinciding on the x-axis where ΔpH is zero at initial pH represents the PZC.

Optimization of adsorption parameters (batch experiment)

The batch experiment was carried out by varying adsorption parameters, such as the ppm concentration of the sorbent, contact time (30–150 min), temperature (20–50 °C), pH (3–11), and adsorbent dosage (0.5–2.5 g). For this purpose, a 1000 mL round-bottom flask was taken, and 1 g of crystal violet was used to prepare a 1000 ppm stock solution for dye. The stock solution was adjusted to the mark. This dye stock solution was used to prepare varying concentrations of crystal violet, such as 20, 40, 60, 80, and 100 ppm. These solutions were used in the adsorption batch experiment to check the adsorption potential of adsorbents. Then, Erlenmeyer flasks (250 mL) were used, which could accommodate 100 mL dye solution. An orbital shaker (SHIN SAENG, Model No. SKIR-601L) was used to run each solution at 120 rpm. After running the solution with adsorbent, the UV-visible spectrophotometer (Peak Instruments Model No. C-7200, Peak Instruments (Shanghai) Co., Ltd. China) was used to check the residual crystal violet concentration at the λ_{max} (590 nm). The following equation was used to calculate the adsorption efficiency ($R\%$), where C_o represents the initial concentration of crystal violet, and C_e is the equilibrium concentration of crystal violet:

$$R\% = \frac{C_o - C_e}{C_o} \times 100$$

The following equation was used to determine the potential of crystal violet dye (q_e, mg g^{-1}) to be adsorbed on the adsorbent's surface at equilibrium. Here, V stands for the volume of crystal violet solution in liters (L), and m (g) is the mass of the sorbents, $i.e.$, DO/S and DO/S NPs.[18]

$$q_e = \frac{C_o - C_e}{m} \times V$$

To calculate the amount (q_t, mg g^{-1}) of crystal violet adsorbed onto DO/S and DO/S NPs at a specific time (t), the following equation was employed:[19–21]

$$q_t = \frac{C_o - C_t}{m} \times V$$

All the experimental data were analyzed with the help of Origin Pro 2022 Version Number 225 (9.9.0.225). Moreover, different adsorption isotherms were employed. In the kinetic experiment, 80 ppm was set for both adsorbents, whereas the time of 30 minutes was set for DO/S and 90 minutes for DO/S NPs. However, the experiment volume was set at 100 mL, although the fixed doses of DO/S and DO/S NPs were 0.5 g and 1 g. During the experiment, 10 mL of suspension was taken out at various intervals and subjected to orbital shaking to determine the residual concentration of crystal violet in the solution. In addition, the adsorption kinetics of crystal violet were evaluated by employing a first-order kinetic model.

Adsorption thermodynamics

The effect of temperature on the adsorption process was determined by performing the experiment within a range of temperatures (293.15 to 323.15 K). Adsorption experiments were performed at different temperatures ranging from 20 to 50 °C with a dye concentration of 80 ppm and adsorbent amounts of 0.5 g (with DO/S) and 1 g (with DO/S NPs). Thus, we obtained enough experimental data for analysis.

Adsorption kinetics

In this study, the adsorption statistics were evaluated by using the pseudo-first-order and pseudo-second-order kinetic models.

Adsorption isotherms

Adsorption isotherms were used to explain the interaction of the adsorbate (dye) molecules with the adsorbent until they reached the equilibrium state.

Result and discussion

Characterization of adsorbents by various techniques

The two adsorbents DO/S and DO/S NPs were characterized by different analytical techniques to evaluate the presence of functional groups, elemental composition, thermal stability, and morphology. Moreover, a comparison of both adsorbents was made based on the containerization results.

Fourier transform infrared (FTIR) spectroscopy

The FTIR spectra of crystal violet are shown in Fig. 2. The cationic crystal violet dye shows the characteristic peaks of 151.19 cm^{-1} due to the C=C stretching vibrations in the atomic nuclei, 1309.67 cm^{-1} due to C–H distortion in the methyl group, 2989.66 cm^{-1} due to the stretching vibration of sp^3 hybridization (–C–H–), and a peak at 3797.84 cm^{-1} due to the O–H bonds of adsorbed water molecules on the surface of the crystal violet dye. The peaks of DO/S that appear before adsorption are quite different from those that appear after adsorption of crystal violet, as shown in Fig. 2. There is a visible shift in the peaks after the adsorption of dye onto de-oiled *Glycine max* L. The
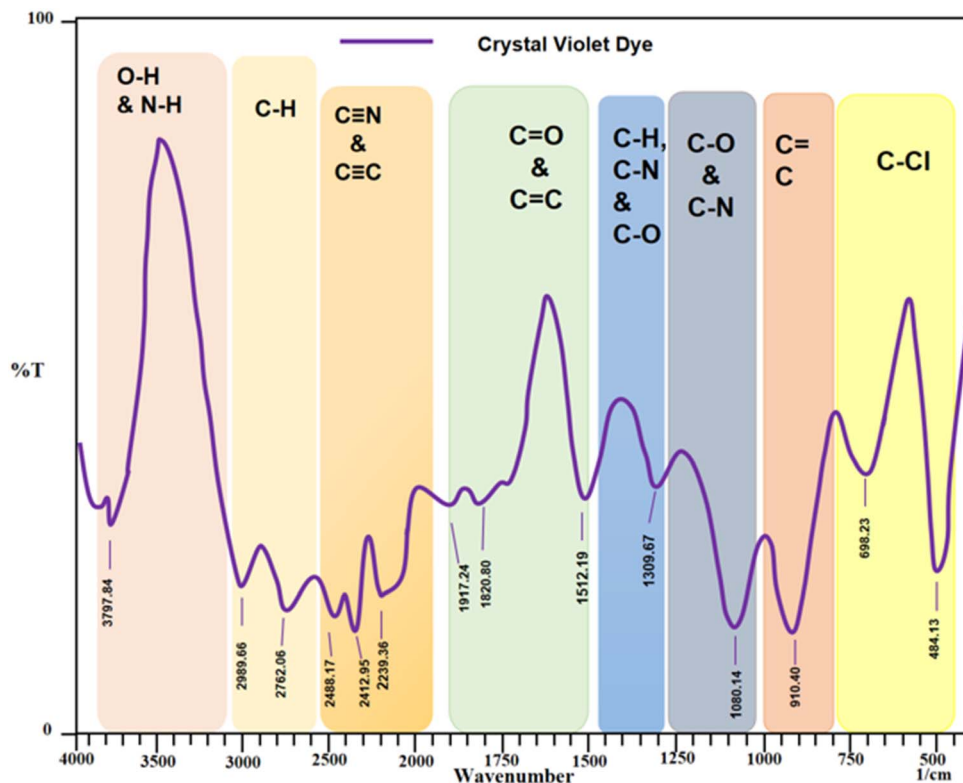
Fig. 2 FTIR spectra of crystal violet.

peak from the C–H stretching vibrations of sp^3 hybridized carbon (–C–H–) shifted from 2906.73 cm^{-1} to 2904.80 cm^{-1}. The peak corresponding to the C≡N groups shifted from 2241.28 cm^{-1} to 2233.57 cm^{-1}, which indicates the formation of a new bond. This peak causes the new stretching vibrations attributed to the CH$_3$, CH$_2$, and CH groups.[22] An intense peak shift from 1697.37 cm^{-1} to 1720.50 cm^{-1} shows the interaction of the C=O group with adsorbed dye molecules. Moreover, the shift of 3541.31 cm^{-1} to a broader peak of 3649.32 cm^{-1} is due to the adsorbed O–H groups on the surface. The C–O bond stretching mode in esters, ethers and phenols at 1055.06 cm^{-1} shifted to 1197.79 cm^{-1} after the adsorption of crystal violet. The emergence of a new peak at 2233.57 cm^{-1} indicates the C≡N stretching vibration present in crystal violet (Fig. 3a).

The peaks for DO/S NPs before and after the adsorption of crystal violet are different, as shown in Fig. 3a. Before adsorption, the peaks at 3473.80 cm^{-1} and 3415.93 cm^{-1} show the presence of phenolic groups present in the seed. Moreover, the peak at 1687.1 cm^{-1} is due to the C=O stretching of ketone and acids. The presence of peaks at 653.87 cm^{-1} and 567.07 cm^{-1} confirms the presence of CuO NPs. This shows that the biological nature of the seeds has a dual functionality of stabilization and CuO NPs formation.[5–7]

There is a prominent shift in the peaks that occurs after the adsorption of crystal violet onto the surface of DO/S NPs. The shift of peaks from 3415.93 cm^{-1} and 3473.80 cm^{-1} to 3466.08 cm^{-1} and 3604.96 cm^{-1} is due to the adsorbed O–H groups onto the surface of DO/S NPs. The peak corresponding to

the C–H stretching vibrations of the sp^3 hybridized (–C–H–) shifted from 2910.58 cm^{-1} to 2866.22 cm^{-1}. Another intense peak appears when the C=N groups shifted from 2264.43 cm^{-1} to 2233.57 cm^{-1}, which shows the formation of a new bond that leads to the stretching vibrations of the CH, CH$_2$, and CH$_3$ groups.[1] An intense and broad peak shift from 1687.71 cm^{-1} to 1716.65 cm^{-1} shows the interaction of the C=O group in the adsorbent with the adsorbed dye molecules (Fig. 3b).

Scanning electron microscopy (SEM)

SEM analysis was performed to obtain information about the space accessible for adsorption and the morphology of the adsorbent material (Fig. 4 and 5). In this strategy, the surface of the adsorbent is characterized *via* light emission. This analytical technique is especially used to take high-resolution images of synthesized nanoparticles even below 10 nm. Results showed that the surface of the synthesized nanoparticles was smooth, along with cavities that facilitated crystal violet adsorption. Spherical structures were also observed, along with irregularities in the morphological view from different angles, as shown in Fig. 6. The literature has also shown similar SEM results for copper nanoparticles.[8,23]

Energy dispersive X-ray (EDX)

EDX analysis was performed to obtain in-depth knowledge of the elemental composition of the synthesized loaded nanoparticles on de-oiled *Glycine max* L., as given in Fig. 7.
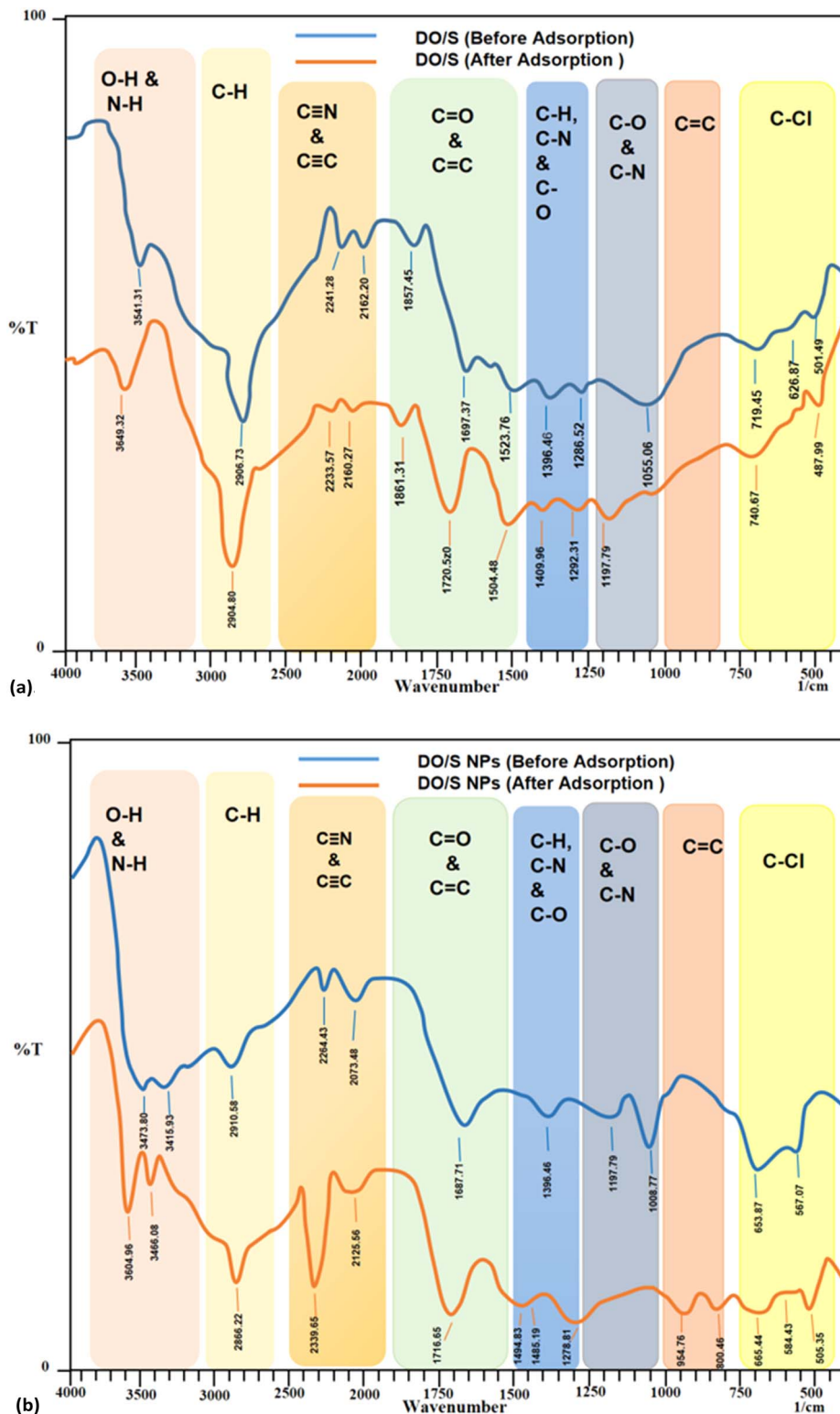
Fig. 3 (a) FTIR spectra of de-oiled *Glycine max* L. (before and after adsorption). (b) FTIR spectra of de-oiled *Glycine max* L. loaded with Cu NPs (before and after adsorption).

The EDX spectrum of DO/S NPs showed the presence of Cu, which indicated the synthesis of the desired copper nanoparticles. Therefore, the detection of copper indicates that the copper nanoparticles have been successfully introduced and possibly attached to or incorporated within the *Glycine max* L. seed material.[9] The presence of oxygen along with copper could suggest partial oxidation of the copper nanoparticles, forming copper oxides (CuO, Cu_2O). Carbon is a key element in the
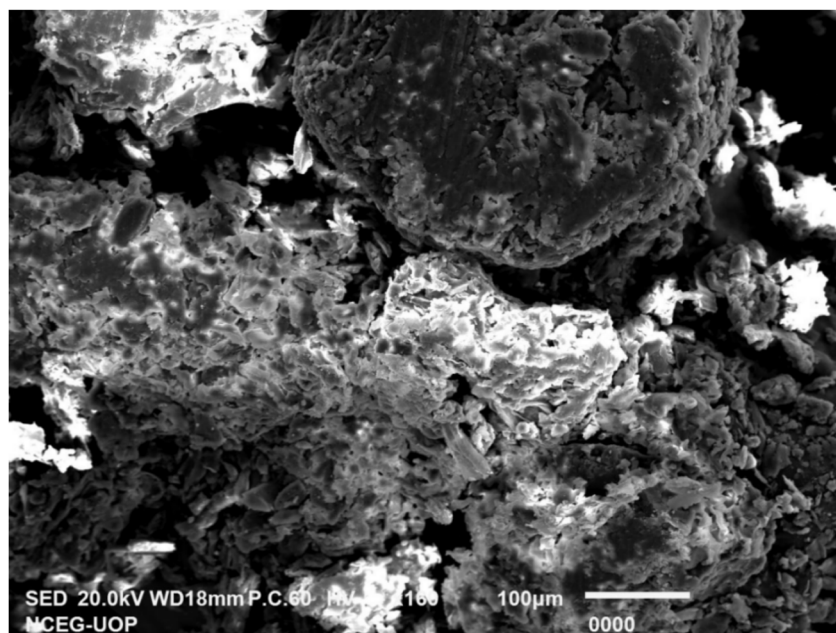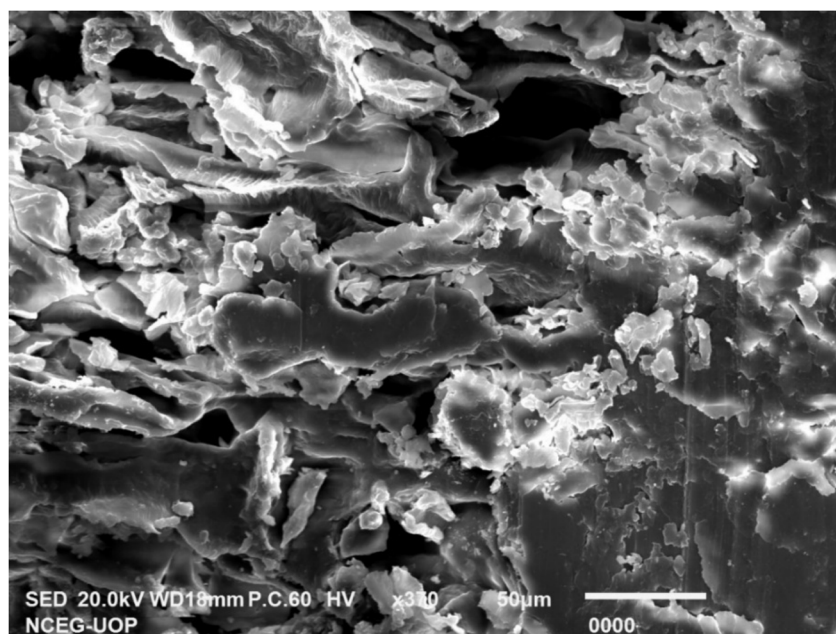
Fig. 4 SEM of DO/S NPs at 100 μm and ×160 magnification.

Fig. 5 SEM Of DO/S NPs at 50 μm and ×370 magnification.

organic structure of *Glycine max* L. seeds, and may also come from organic capping or stabilizing agents used in nanoparticle synthesis. The presence of C and O peaks showed that carbon-based stabilizers must be present.[10]

Point of zero charge (PZC)

The salt addition method was used to evaluate the point of zero charge of the DO/S and DO/S NPs. In this method, 500 mL of 0.1 M of sodium nitrate solution was prepared in the flask.

From this solution, 50 mL was taken out and transferred to 10 different conical flasks. The pH (3–11) was adjusted in each flask using HCl and NaOH, with each at 0.1 M. After adjusting the pH value, 1 g DO/S was added to the five flasks, and DO/S NPs were introduced into the other five flasks containing the solutions of varying pH levels.

Then, these solutions were ready to go through the 24 hours of agitation in the orbital shaker. After completion of the reaction, the solutions were filtered and the change in pH was carefully checked with a pH meter.[16,19]
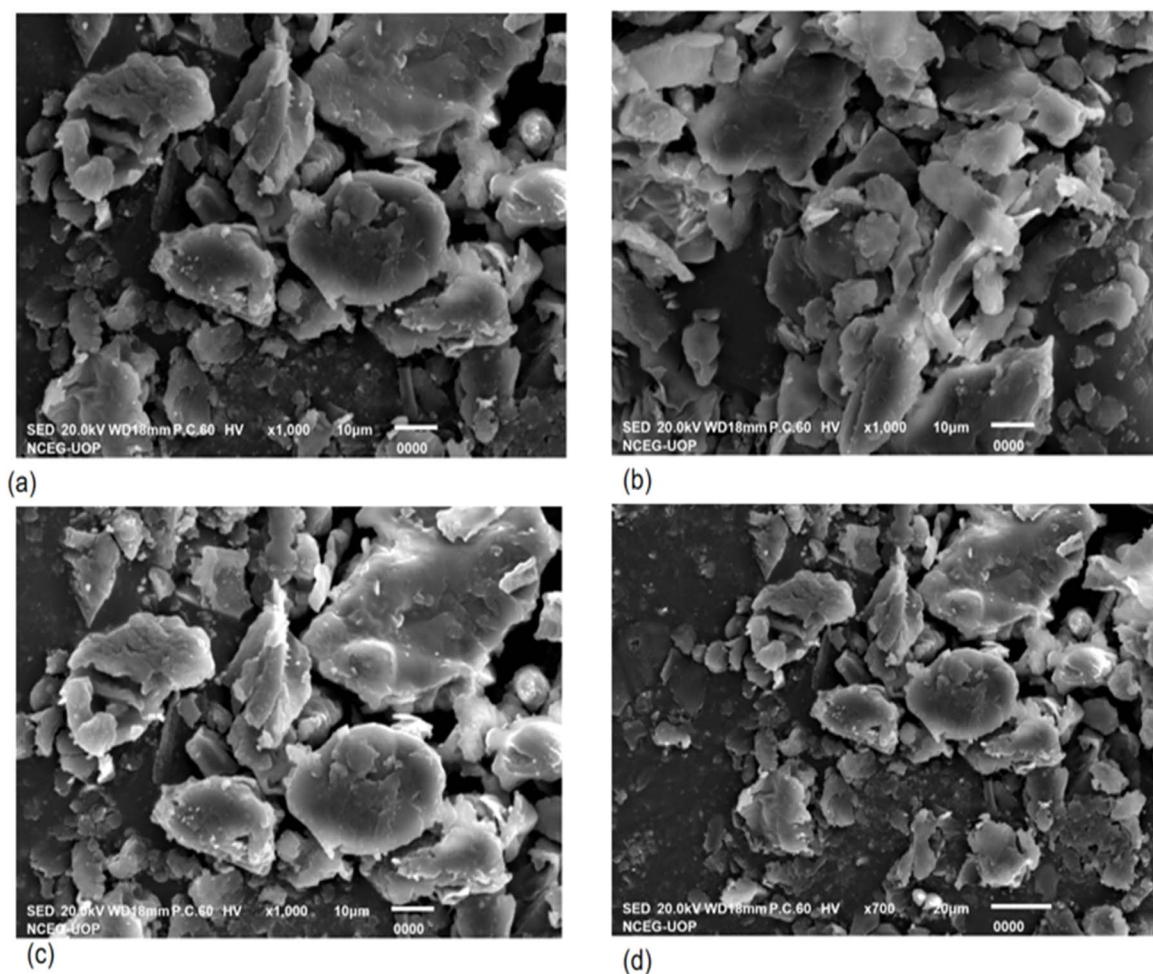
Fig. 6 SEM Of DO/S NPs at different scale bars and magnifications: (a) 10 μm, ×1000; (b) 10 μm, ×1000; (c) 10 μm, ×1000; and (d) 20 μm, ×700.

The following equation was used to compute the altered pH, where pH_o is the initial pH before agitation, and pH is the final pH after agitation.

$$\Delta pH = pH_o - pH$$

The ΔpH was plotted against the initial pH values to evaluate the PZC. The point coinciding on the x-axis where ΔpH is zero at the initial pH represents the PZC.

The point of zero charge results for DO/S and DO/S NPs are given in Fig. 8. Therefore, the adsorbents, *i.e.*, DO/S and DO/S NPs, have zero charges at the surface when the pH of the solution is 6.7 and 7.7. When the surface of the adsorbent is negatively charged (pH > PZC), the adsorption of cationic dyes is favorable. Conversely, when the sorbent's surface acquires a positive charge (pH < PZC), efficient adsorption of anionic dyes is facilitated.[11–13] Subsequently, in the case of DO/S as an adsorbent, adsorption is more efficient in neutral and basic conditions (7, 9, and 11 pH) towards crystal violet. In the case of DO/S NPs as an adsorbent, basic conditions (9, 11 pH) facilitate excellent crystal violet removal.

Thermogravimetric analysis (TGA)

Thermogravimetric analysis of de-oiled *Glycine max* L. and de-oiled *Glycine max* L. loaded with CuO nanoparticles was performed to calculate the weight loss percentage using temperature and time functions. Fig. 9 and Table 1 show the gradual loss of weight from 26.59 °C (room temperature) to 221.94 °C because of volatile content like moisture in the DO/S. On further increase of temperature to 446 °C, major weight loss occurs mainly due to the pyrolysis of *Glycine max* L. (DO/S). In the case of DO/S NPs, the slight change in weight loss occurs due to water evaporation at 244.03 °C. Major weight loss occurs at 467.47 °C due to the decomposition of loaded CuO nanoparticles and the pyrolysis of the *Glycine max* L.[14,15,24]

Brunauer–Emmett–Teller (BET) analysis

For surface characterization of the adsorbent, BET analysis was performed, and the surface area of the adsorbent, pore volume, and diameter of the surface pores were calculated. Results reveal that the BET surface area of the nanoparticles was 101.1 m^2 g^{-1}, while the pore diameter and micropore volume were 0.411 nm and 0.040 cm^3 g^{-1}, respectively. Fig. 10 shows the N_2 adsorption and desorption isotherm, which is a type IV type

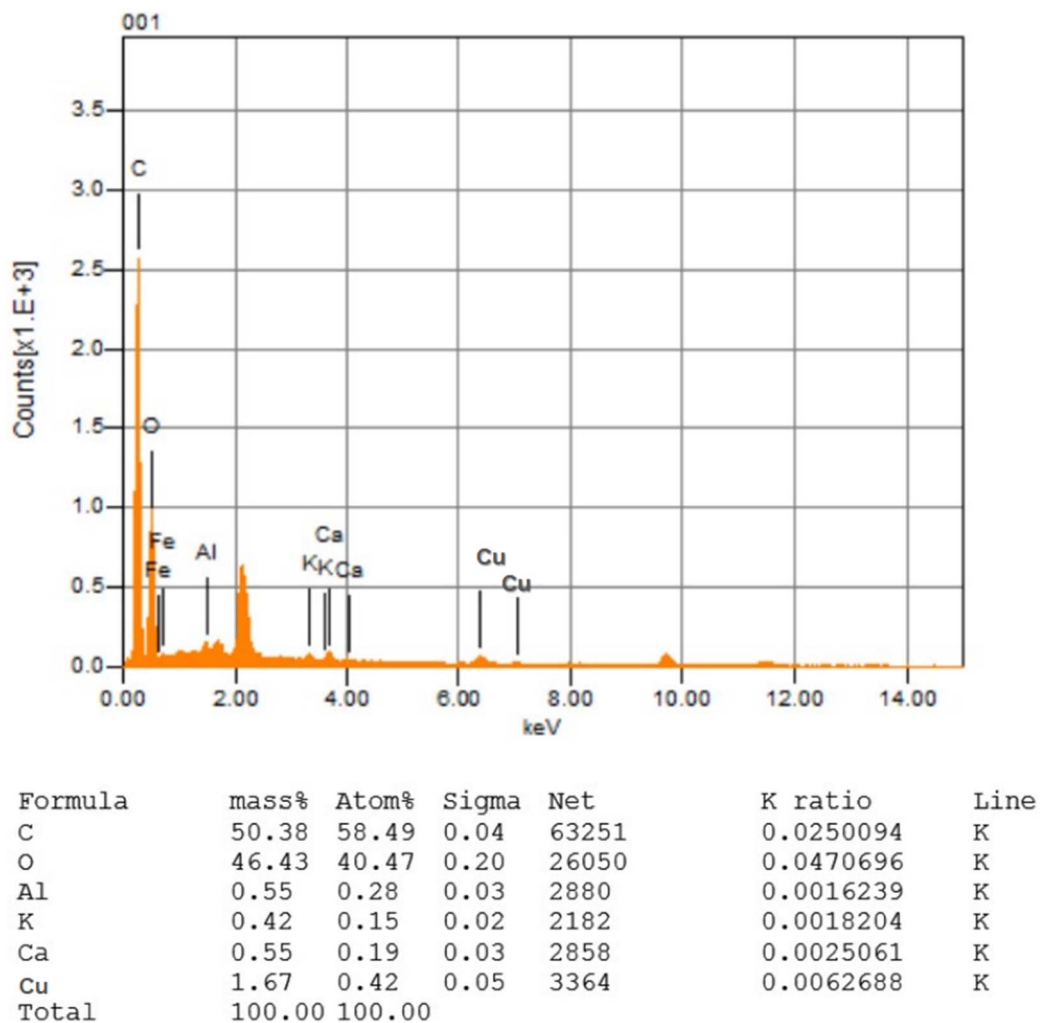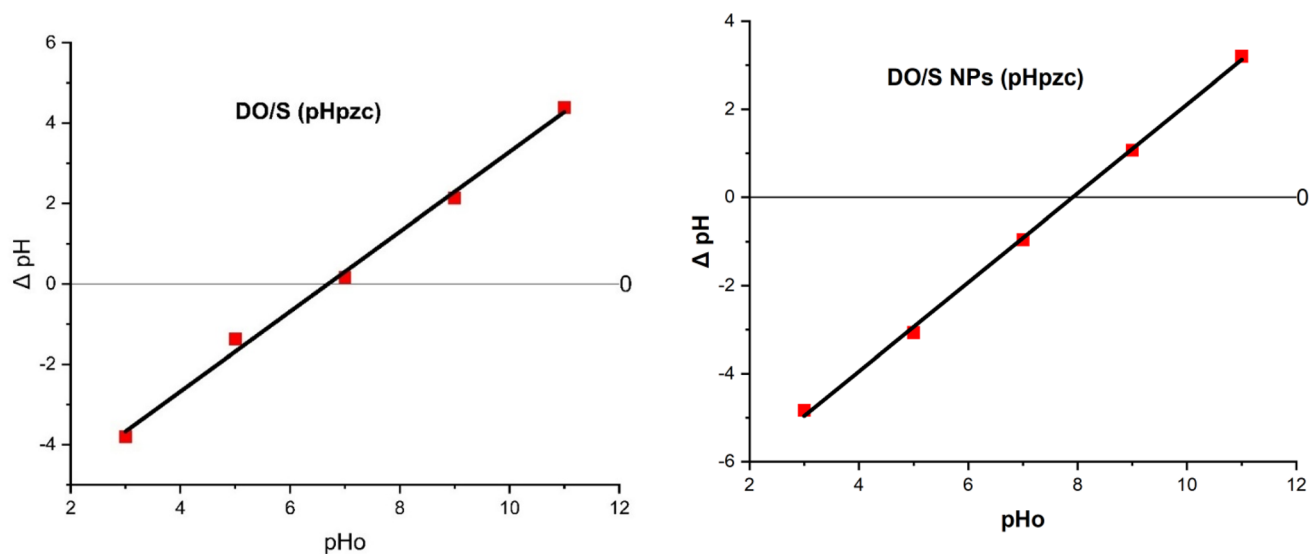| Formula	mass%	Atom%	Sigma	Net	K ratio	Line
C	50.38	58.49	0.04	63251	0.0250094	K
O	46.43	40.47	0.20	26050	0.0470696	K
Al	0.55	0.28	0.03	2880	0.0016239	K
K	0.42	0.15	0.02	2182	0.0018204	K
Ca	0.55	0.19	0.03	2858	0.0025061	K
Cu	1.67	0.42	0.05	3364	0.0062688	K
Total	100.00	100.00				

Fig. 7   EDX results of DO/S NPs.
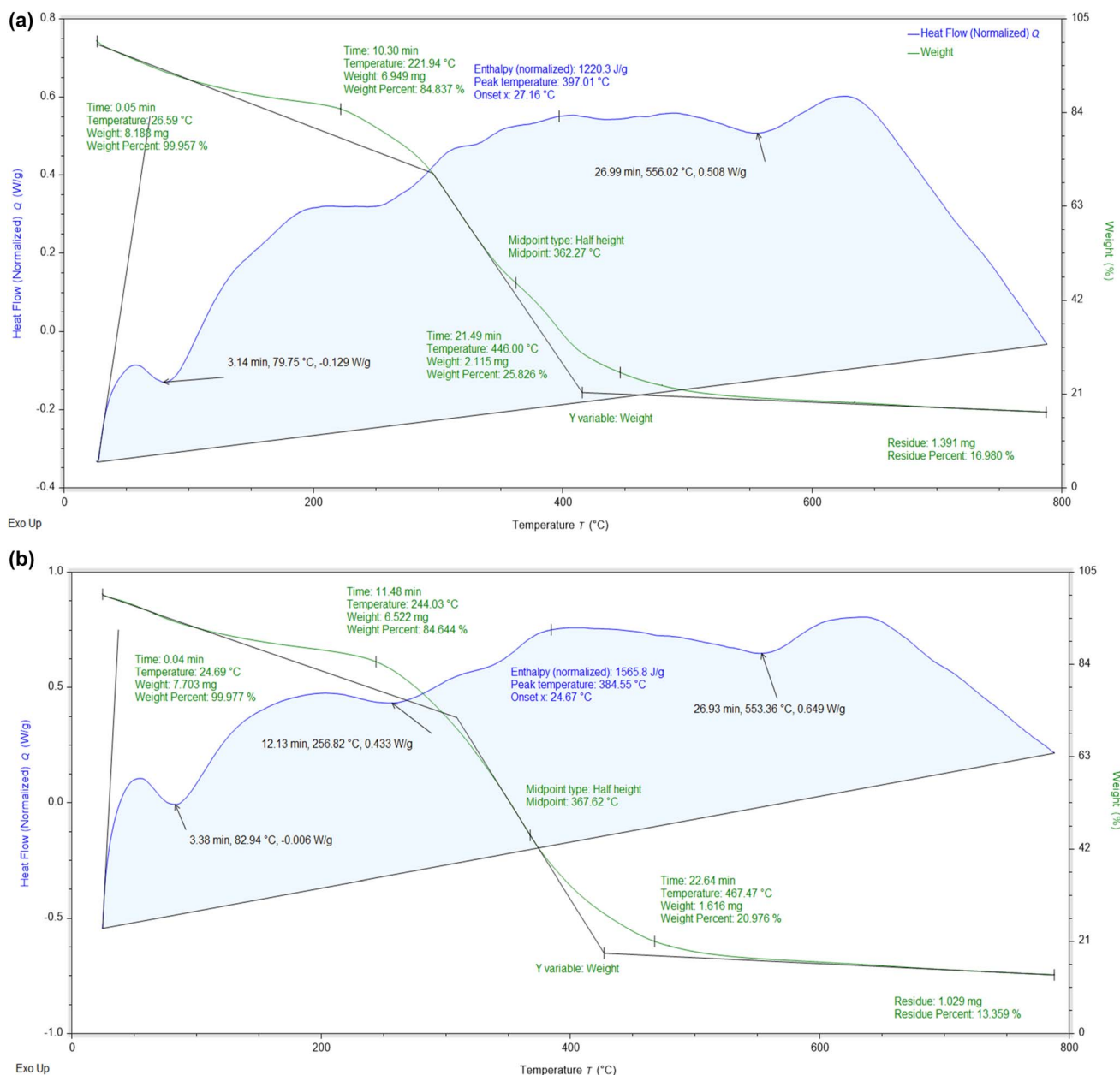

Fig. 8   pH PZC determination of DO/S and DO/S NPs.

Fig. 9 TGA results of (a) DO/S and (b) DO/S NPs.

Table 1 TGA results of DO/S and DO/S NPs

Time	Temperature	Weight	Weight percent
DO/S			
0.05 min	26.59 °C	8.188 mg	99.957%
10.30 min	221.94 °C	6.949 mg	84.837%
21.49 min	446.00 °C	2.115 mg	25.826%
DO/S NPs			
0.04 min	24.69 °C	7.703 mg	99.977%
11.48 min	244.03 °C	6.522 mg	84.644%
22.64 min	467.47 °C	1.616 mg	20.976%

of isotherm with a hysteresis loop. Materials with pore diameters in the range of 2–50 nm usually give this type of curve. The results support the formation of nanoparticles, as well as it being a well-suited method for adsorption.

Optimization of adsorption parameters

Adsorption of crystal violet dye was performed at variable parameters, including the initial concentration of dye, time, temperature, pH, and amount of adsorbent used, as given in Fig. 10. The purpose of the parameter optimization is to obtain
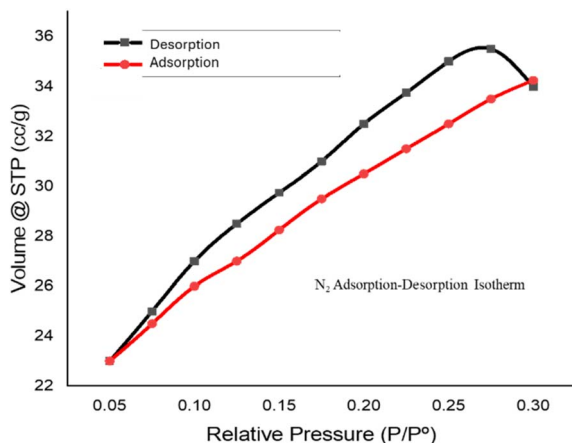
Fig. 10   BET plot for the nanoparticles.

a suitable combination of different variables for the best adsorption of dye.

Effect of initial concentration of crystal violet

The efficient removal of crystal violet increases with an increase in concentration. In the case of DO/S, at 80 ppm, the removal rate reaches the maximum level of 88.92%. The percentage removal does not increase after this concentration due to the occupation of active sites on the absorbent. This trend indicates that the DO/S adsorbent has many vacant positions. However, as the crystal violet concentration reaches 80 ppm concentration, the adsorbent becomes saturated.[25] Thus, no visible enhancement of adsorption activity is observed beyond 80 ppm.

In the case of DO/S NPs, at 80 ppm, the dye removal rate is at its highest level of 94%. Furthermore, an increase in dye concentration does not increase the adsorption rate because there is no active site left vacant. However, further increase leads to a decrease in the adsorption rate. This decline occurs due to the saturation of adsorption sites when dye molecules start accumulating in the solution. The amount of dye adsorbed per unit mass of the adsorbent ($mg\ g^{-1}$) increased as the initial dye concentration rose. This occurred due to the adsorbent's resistance to any further uptake of dye molecules from the aqueous solution as the concentration increases.[26] Besides this, a clear comparison of the removal efficiency between the de-oiled *Glycine max* L. seed and de-oiled *Glycine max* L. loaded with Cu NPs is shown in Fig. 10. The graph shows the visible enhancement in percentage sorption by seeds after being loaded with copper oxide nanoparticles.

Effect of contact time

The duration of an adsorption process is heavily influenced by the contact time between the adsorbent and the adsorbate. This parameter is vital as it offers insights into the sorption kinetics of the adsorbate. The effective removal of crystal violet is directly related to the contact time until it reaches equilibrium. In the case of DO/S, the maximum removal rate (91%) is attained at 30 min. From Fig. 10, the absorption of crystal violet

decreases after 30 minutes, and then a sudden rise is observed at 90 minutes. However, the decline in adsorption rate occurs again after 120 minutes. So, another experiment was performed at 30 minutes with the DO/S. Whereas in the case of DO/S NPs, the dye removal rate (95%) is highest at 90 min. At this particular time, the equilibrium is achieved and a further increase in contact time will be of no use.[22] Fig. 10 shows that the adsorption reaches its maximum level at 90 min. However, the adsorption rate becomes constant after 90 minutes. This indicates that the DO/NPs adsorbent has achieved the equilibrium level. Thus, further experiments were performed at 90 minutes with the DO/S NPs. The graph between the percentage sorption and time depicts the comparison between the de-oiled *Glycine max* L. and the de-oiled *Glycine max* L. loaded with the CuNPs, as shown in Fig. 10.

Effect of temperature

The removal rate of crystal violet increases with the temperature rise. This trend is the result of an increase in the kinetic energy, which facilitates dye adsorption. Also, in both cases, *i.e.*, DO/S and DO/S NPs, the maximum adsorption rate is achieved at 293.15 K. Beyond this specific temperature, the experiments have not shown any further rise in the sorption rate. However, Fig. 10 shows the decline in the adsorption rate of crystal violet on a further increase in temperature. This suggests that the adsorption of crystal violet onto both adsorbents is an exothermic process. The same behavior is also shown in the physical adsorption processes. Thus, the temperature rise lessens the interaction of crystal violet molecules and adsorbent, leading to desorption.[27] Moreover, the apparent difference in crystal violet dye removal by the two adsorbents is shown in Fig. 10.

Effect of pH

The chemical makeup of the adsorbent and adsorbate is related directly to the rate of adsorption. These characteristics may vary with varying pH. In the case of DO/S, the highest removal rate of crystal violet from aqueous media is attained at a pH of 7. Therefore, the most efficient adsorption will occur if there is a neutral medium, *i.e.*, strong attractive forces between the adsorbent and dye. Whereas in the case of DO/S NPs, the maximum adsorption of cationic crystal violet is achieved at a pH value of 9 (basic medium), as supported by the zeta potential. Thus, at pH values above PZC, the adsorbent will acquire a negative charge and will be more attracted toward the positively charged crystal violet molecules. However, with the decrease in pH, there will be weaker electrostatic forces between the adsorbent and dye molecules due to the same charges (positive charges). Experimental data in the literature related to crystal violet removal also support the present study.[28]

Effect of the amount of adsorbent

The adsorption of crystal violet dye increases with the increase in the dose of prepared adsorbent. In the case of de-oiled *Glycine max* L. seeds, the removal rate reaches the maximum level of 91% at 0.5 g. Any further increase in the concentration

follows the trend of decreasing percentage sorption. This occurs due to the overloading of the adsorbate molecules over the adsorbent, which leads to reduced active sites. In the case of de-oiled *Glycine max* L. seeds loaded with Cu NPs, the removal rate is highest (95%) at 1 g of adsorbent. Any further increase in dose slows the adsorption process and decreases the removal rate of crystal violet. The reduction in adsorption capacity with increasing adsorbent dosage may be attributed to the aggregation of adsorbent particles at higher doses. This aggregation can block some of the active sites on the adsorbent surface which causes a significant decrease in the overall adsorption capacity. The same trend is observed in the effect of varying doses on the dye adsorption in the previous literature.[29,30] However, the graph between the percentage sorption and the amount of dose shows a clear analogy of DO/S and DO/S NPs, as shown in Fig. 10.

Thermodynamics

To determine the spontaneity, randomness, or exo- and endo-thermal property during the adsorption process, thermodynamics studies are essential. Moreover, the pattern of the adsorption mechanism can also be determined by thermodynamic parameters. $\Delta G°$, $\Delta H°$, and $\Delta S°$ can be calculated by the following equations.

$$\Delta G° = -RT \ln K_d$$

$$\Delta G° = \Delta H° - T\Delta S°$$

The values of $\Delta H°$ and $\Delta S°$ for the adsorption of crystal violet onto the de-oiled *Glycine max* L. and CuO-loaded de-oiled *Glycine max* L. can be obtained from the van't Hoff equation:

$$\ln K_d = \frac{\Delta S°}{R} - \frac{\Delta H°}{RT}$$

The value of K_d can be determined by using the following equation:

$$K_d = \frac{q_e}{C_e}$$

K_d = distribution constant for the sorption process, R = gas constant, T = absolute temperature (K), $\Delta G°$ = Gibb's free energy, $\Delta H°$ = enthalpy change, $\Delta S°$ = entropy change, where 'q_e' (mg g^{-1}) and C_e (mg L^{-1}) are the amount of crystal violet dye adsorbed onto DO/S and DO/S CuNPs at equilibrium and the equilibrium concentration of crystal violet dye in solution, respectively. The values of enthalpy change and entropy change during the process ($\Delta H°$ and $\Delta S°$) are obtained from the slope and intercept of the linear graph plotted as $1/T$ *vs.* $\ln K_d$. In this present study, the experimental data collected at various temperatures ranging from 293 K to 323 K are shown in Table 2.

According to the results, in the case of DO/S (de-oiled *Glycine max* L.), $\Delta G°$ is negative at 293 K, indicating the spontaneous nature of adsorption. However, with the temperature rise, the positive value of $\Delta G°$ increases, which turns the adsorption into

Table 2 Thermodynamics results for crystal violet dye adsorption

Parameters	Thermodynamics model		Crystal violet dye	
	Temp. (°C)	Temp. (K)	DO/S	DO/S CuNPs
$\Delta G°$ (kJ mol^{-1})	20	293.00	−0.1128	−2.4864447
	30	303.00	0.0451	−2.33073
	40	313.00	0.2009	−1.85377
	50	323.00	0.2059	−1.85998
$\Delta H°$ (kJ mol^{-1})	Calculated from slope		−3.4005	−9.4503
$\Delta S°$ (J K^{-1} mol^{-1})	Calculated from intercept		−11.3161	−23.7586
R^2			0.8514	0.8893

a non-spontaneous reaction. Moreover, the negative value of $\Delta H°$, *i.e.*, −3.4005, indicates the exothermic nature of the reaction and the domination of the van der Waals forces.[31] In addition, the negative value of $\Delta S°$ indicates that there is less randomness during adsorption. In the case of DO/S NPs, all of the values of $\Delta G°$ are negative, which indicates the spontaneous and favorable adsorption reaction. Similar results have also been reported on the adsorption of crystal violet by coffee husks and date palm fiber.[32,33] Moreover, the negative values of $\Delta H°$ and $\Delta S°$ show the exothermic nature and randomness during adsorption, respectively.

Adsorption isotherms

Adsorption isotherms and calculations result in equilibrium data used to verify the functionality of the whole process. Additionally, they forecast how the contact mechanisms will work in various operational scenarios. Numerous adsorption isotherms can be found in this sense. In the present investigation, a few were selected—Langmuir, Freundlich, Temkin, and D–R isotherm, and discovered to be very appropriate.

The results show that all the adsorption isotherms have a high R^2 value of 0.9, except for the Freundlich and Langmuir isotherms, as listed in Table 3.

Freundlich adsorption isotherm

The multilayer nature of the adsorption process is identified by the Freundlich isotherm. Freundlich constants K_F and $1/n$, respectively, indicate the adsorption intensity and capacity. For adsorption, a value of K_F between 1 and 20 is deemed favorable. Similarly, a low value of $1/n$ indicates a heterogeneous surface that is appropriate for adsorption. Based on the Freundlich constants, the study's results demonstrate the effective adsorption in the case of DO/S NPs as the value of K_F increases, which indicates the enhancement in the adsorption capacity. Moreover, after loading the CuO nanoparticles, the value of $1/n$ decreases, which signifies effective adsorption. Therefore, a comparison of the results (K_F and $1/n$) shows that crystal violet was adsorbed more favorably with DO/S NPs than with DO/S.

Table 3 Calculations of adsorption isotherms

Adsorption isotherm models	Crystal violet dye (linear form)	
Freundlich	DO/S	DO/S Cu NPs
K_F (mg g^{-1})	8.4793×10^{-8}	0.11156
$1/n$	7.8508	2.51435
R^2	0.81	0.82

Adsorption isotherm models	Crystal violet dye (linear form)	
Langmuir	DO/S	DO/S Cu NPs
R_L	−0.0046	−0.0066
q_m (mg g^{-1})	0.0417	0.3863
K_L	−10.8977	−7.588
R^2	0.7	0.73

Adsorption isotherm models	Crystal violet dye (linear form)	
Dubinin–Radushkevich	DO/S	DO/S Cu NPs
q_{mDR} (mg g^{-1})	332.2839917	23.60645048
K_{DR} (mol^2 kJ^{-2})	7.09×10^{-5}	5.90×10^{-6}
R^2	0.90	0.93
E (kJ mol^{-1})	0.0840	0.2911

Adsorption isotherm models	Crystal violet dye (linear form)	
Temkin	DO/S	DO/S NPs
K_T	0.123380601	0.35905
R^2	0.9	0.91
B_T (J mol^{-1})	31.43	11.90803

Langmuir adsorption isotherm

The unilayer adsorption phenomena are the underlying premises of the Langmuir model. The maximum monolayer adsorption capacity is obtained with constant q_m. However, the Langmuir affinity parameters are obtained from the Langmuir constants R_L. The maximum adsorption is represented by a large value of q_m, and adsorption is deemed effective when the R_L value is low. According to the results of the Langmuir isotherm in Table 3, the value of q_m increases and R_L decreases after the loading of copper oxide nanoparticles on the adsorbent. Therefore, compared to DO/S, DO/S NPs demonstrate the more effective dye adsorption of crystal violet.

Dubinin–Radushkevich (D–R) isotherm

The purpose of the D–R model is to identify the type of adsorption reaction. The D–R model suggests whether the nature of the adsorption reaction is physical, chemical, or an ion exchange mechanism. For this model, if the value of E is computed as between 8 to 16 kJ mol^{-1}, then the adsorption follows the ion exchange mechanism. However, if the value of E is less than 8 kJ mol^{-1}, then the physical nature of adsorption is confirmed. An adsorption process is a chemisorption if the E value is more than 16 kJ mol^{-1}. The present investigation yields a notably low value of E with both adsorbents (DO/S and DO/S NPs), confirming the physisorption of the adsorbent surface.

Temkin adsorption isotherm

The Temkin isotherm has a foundation on the concept that the reaction's heat changes along the way in the whole process (Fig. 11 and 12). Information regarding the binding energy during the adsorption process can be acquired by the Temkin constant (K_T). However, the constant B_T gives data concerning the adsorption heat. The results reported in Table 3 demonstrate that the adsorption reaction employing both adsorbents, DO/S and DO/S NPs, is exothermic, as indicated by $B_T > 0$.

Adsorption kinetics

The adsorption kinetics is a crucial part of the study, and is conducted by applying two adsorption kinetic models. Thus, pseudo-
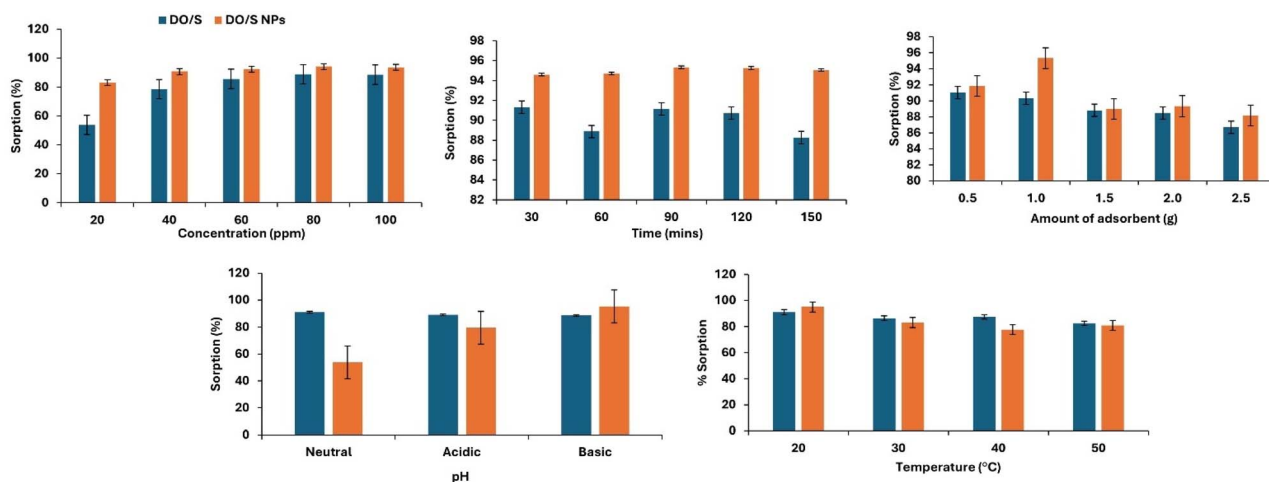

Fig. 11 A comparison of the impacts of concentration, time, adsorbent dose, pH, and temperature on crystal violet adsorption.
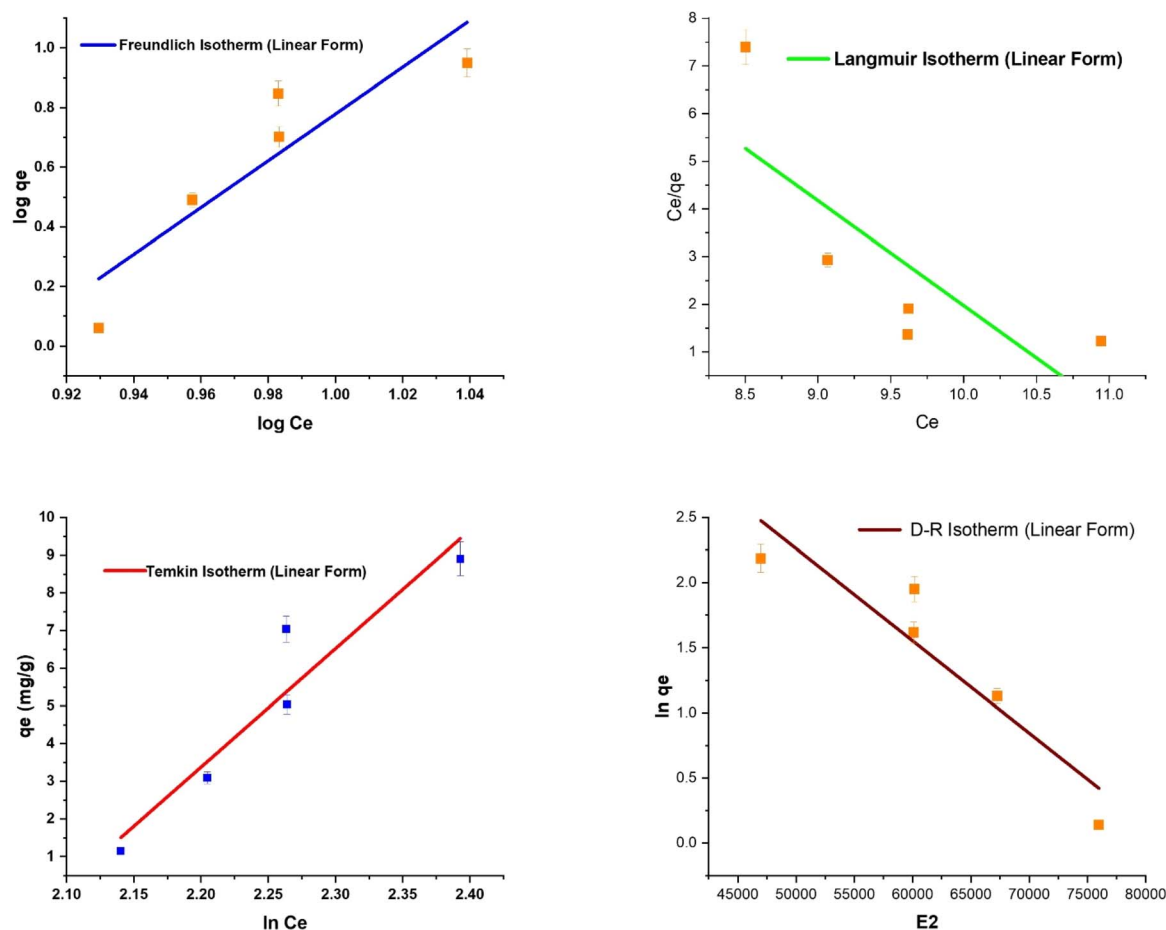
Fig. 12 Linear forms of the Freundlich, Langmuir, Temkin, and D–R isotherms (DO/S).

first-order and pseudo-second-order models were used to obtain information about the adsorption process and rate-limiting step. The kinetics of the adsorption of crystal violet onto the *Glycine max* L. adsorbents (DO/S, DO/S NPs) in an aqueous medium were carried out at varying contact times. Therefore, the adsorption kinetics of crystal violet onto the adsorbents (DO/S and DO/S NPs) was determined by these models. In both cases, the pseudo-first-order kinetic model was not successful, which indicates that the adsorption reaction does not follow the assumption of this model. According to the pseudo-first kinetic model, the concentration of adsorbate and its diffusion over the surface of the adsorbent controls the adsorption process.

The employment of a pseudo-second-order kinetic model efficiently fitted the obtained experimental data. In the case of crystal violet adsorption onto DO/S and DO/S NPs, a high value of R^2 (0.99) was obtained, as shown in Table 4. The pseudo-second-order equation is as follows.

$$\frac{\mathrm{d}q_t}{\mathrm{d}t} = K_2(q_e - q_t)^2$$

Rearranging the above equation gives the following,

$$\frac{t}{q_t} = \frac{1}{K_2 q_e^2} + \frac{t}{q_e}$$

where q_t is the amount of dye adsorbed at time t (mg g^{-1}), q_e (mg g^{-1}) is the amount of crystal violet adsorbed at equilibrium, and K_2 is the rate constant of the pseudo-second-order model (g mg^{-1} min^{-1}). In addition, q_t and K_2 were calculated from the obtained slope and graph. The linear graph fit between the t/q_t and contact time (t) is shown in the graph drawn on the origin in Fig. 13. Moreover, Table 4 shows the values of parameters and correlation coefficients of the pseudo-second-order kinetic

Table 4 Kinetics results for crystal violet adsorption

Kinetics models	Crystal violet dye (linear form)	
Pseudo-first order	DO/S	DO/S NPs
K_2 (g mg^{-1} min^{-1})	**0.3023839**	0.3023839
q_{e1} (mg g^{-1})	**1.3599**	1.3599
R^2	**0.125**	0.125

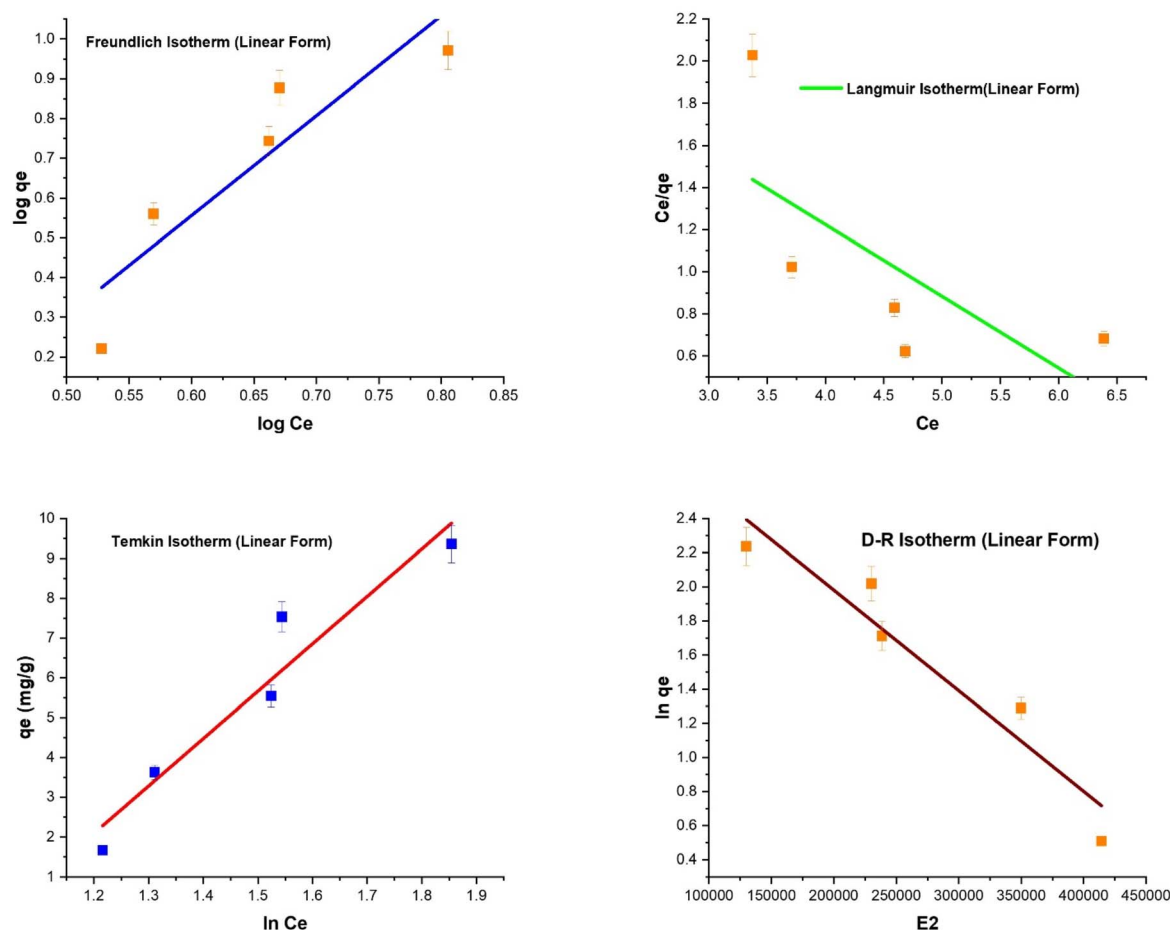| Kinetics models	Crystal violet dye (linear form)	
Pseudo-second order	DO/S	DO/S NPs
K_2 (g mg^{-1} min^{-1})	−0.044648496	0.597712874
q_{e2} (mg g^{-1})	13.67427868	7.534659433
R^2	0.99786	0.99997

Fig. 13 Linear forms of the Freundlich, Langmuir, Temkin, and D–R isotherms (DO/S Cu NPs).

model that best fits the experimental data for both DO/S and DO/S NPs. This means that the adsorption process requires a longer time, and largely depends upon the forces of interaction that are developed between the adsorbate and adsorbent. The results obtained from the kinetic studies were also supported by literature.[34–36]
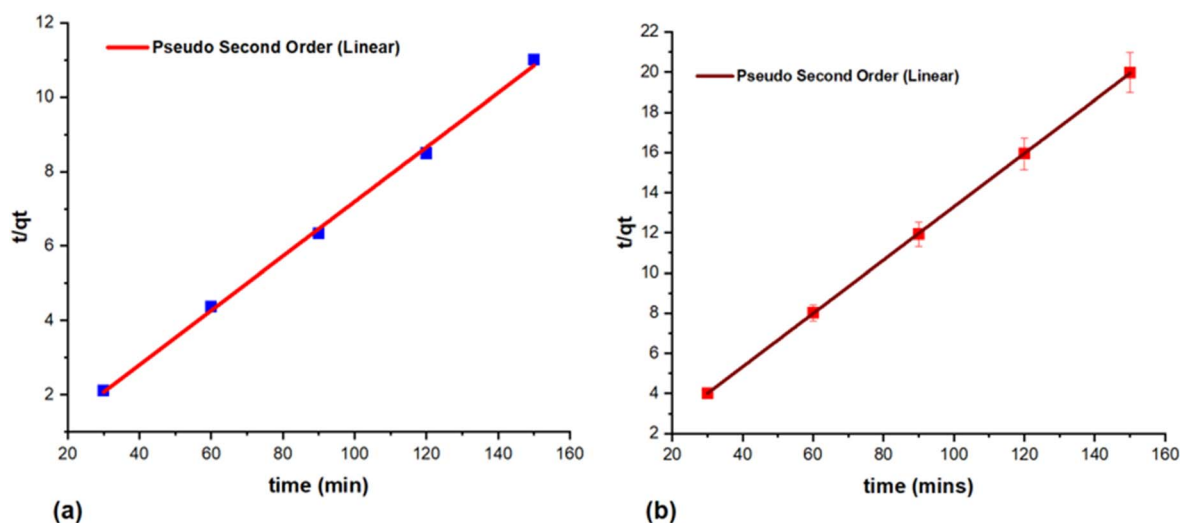

Fig. 14 Kinetic studies on crystal violet using (a) DO/S and (b) DO/S NPs.

Adsorption mechanism

The point of zero charge (PZC) better explains the adsorption mechanism. When the pH of the solution rises above PZC, the adsorbent will become positively charged while facilitating the cationic dye adsorption. On the other hand, the adsorbent will promote anionic dye adsorption when the pH of the solution shows a decline compared to the observed point of zero charge. The PZC (pH at which the surface has zero charge) was calculated for DO/S and DO/S NPs as 6.6 and 6.7, respectively. Therefore, in the case of DO/S as an adsorbent, adsorption is more efficient under neutral and basic conditions (7, 9, and 11 pH) towards crystal violet, which enhances the electrostatic attraction between the cationic crystal violet molecules and the negatively charged adsorbent surface (Fig. 14).

Similarly, with DO/S NPs as an adsorbent, basic conditions (9, and 11 pH) facilitate excellent crystal violet removal, as shown in Fig. 14. The higher value of observed PZC of DO/S NPs revealed that the adsorption process will be facilitated towards crystal violet due to its strong electrostatic attraction over the broad range of pH because the DO/S NPs surface will remain neutral or negatively charged. This electrostatic force of attraction toward crystal violet sheds light on the detailed adsorption mechanism, as shown in Fig. 14. The color change after adsorption is shown in Fig. 15.

Desorption/regeneration studies of nanoparticles

The recovery of the dye-loaded adsorbent can play an eco-friendly and viable role. For this purpose, much research was conducted to analyze the cost-effectiveness and efficiency of the adsorbent.[36–39] The present work demonstrates the recovery of the nanoparticles-loaded adsorbent after the treatment with

ethanol for 2 hours. Desorption was followed by air drying and re-application of the adsorbent for adsorption purposes. Five rounds of experiments were conducted to check the difference in the percentage removal of crystal violet by the adsorbent over the reusable time. Results showed a clear decline (from 91% to 77%) in the adsorption capacity of the adsorbent toward crystal violet in an aqueous medium. The present study showed behavior that was similar to that of other materials used for crystal violet removal. S. K. Shukla *et al.*[40] obtained a removal efficiency above 80% after the regeneration of the adsorbent, along with a 50% retained efficiency up to the 10th cycle (Fig. 16). The drop in efficiency in the present study is primarily attributed to the permanent attachment of some dye molecules to the surface of the adsorbent. FTIR analysis of the DO/S NPs before regeneration, after the original adsorption of CV, shows major shifts in functional groups (Fig. 3b). Specifically, the shifts in the O–H stretching peaks and C–H stretches indicate
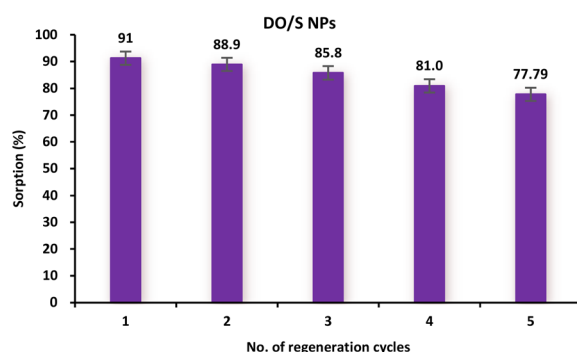

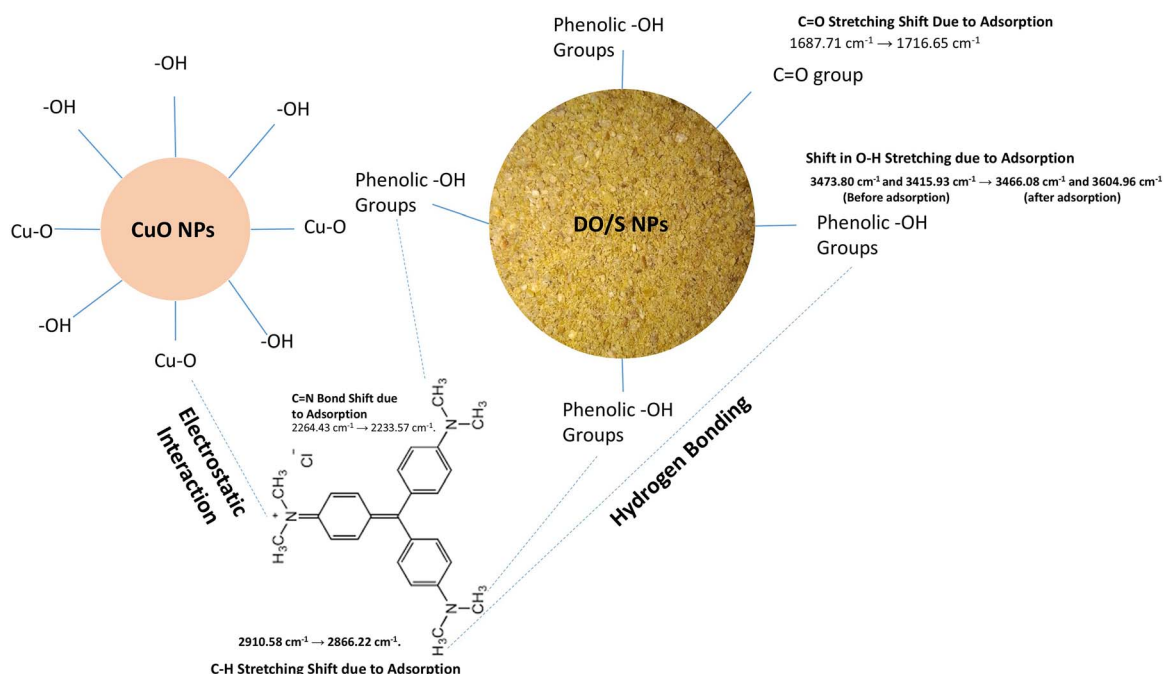**Fig. 16** Regeneration of DO/S NPs for dye removal.

Fig. 15 Adsorption mechanism of DO/S and DO/S NPs.

Table 5 Comparison of DO/S NPs with the existing data

Adsorbent	Adsorbent's dose	Adsorbate (dye)	Adsorption rate	Reference
Glycine max L. seed powder	0.8 g	Methylene blue and malachite green	90%	42
Copper nanoparticles	5 g	Disperse yellow 123 dye	73.50%	43
Copper nanoparticles	0.02 g	Methylene blue	92%	44
DO/S	0.5 g	Crystal violet dye	91%	Present study
DO/S NPs	1 g	Crystal violet dye	95%	Present study

that the dye is adsorbed on the surface, which blocks available active sites. The shift of the C=O stretching peak further confirms that the functional groups on the surface of DO/S NPs bind with the dye molecules. So, the repeated adsorption cycles lead to the blocking of active sites. During regeneration, not all dye molecules are likely to be removed, so active sites are reduced on the surface of the adsorbent. This process of fouling may also contribute to the decline in adsorption efficiency after regeneration.[41] Hence, the regenerated nanoparticles-loaded adsorbent can be used for wastewater treatment due to its excellent reusability.[41]

Comparison of the present study with existing data

To check the potential of the adsorbents, a comparison is made between the present work and previously reported data, as shown in Table 5. According to the literature, *Glycine max* L. powder shows a removal rate of up to 90% of cationic dyes with 0.8 g of adsorbent. Similarly, copper nanoparticles (prepared through green synthesis) achieved maximum azo dye removal of 73.5% with 5 g of adsorbent. However, bio-engineered copper nanoparticles removed 92% cationic dye from the aqueous solution.

Compared with the reported data, the prepared de-oiled *Glycine max* L. seeds showed a removal rate of 91% cationic crystal violet dye with 0.5 g of adsorbent. In addition, the present study showcased the unique strategy of enhancing the adsorbent's capacity by loading it with Cu NPs. Therefore, 1 g of DO/S NPs removed the 95% cationic crystal violet from the aqueous medium, and proved to be a viable and eco-friendly adsorbent.

Conclusions

The present study showed the efficiency of two adsorbents towards crystal violet. The obtained results revealed the improved percentage removal when the adsorbents were loaded with copper nanoparticles. The process was optimized by varying important adsorption factors, such as initial concentration, contact time, pH, adsorbent dose, and temperature. Moreover, various studies, such as isothermal, kinetics, and thermodynamics studies, showed the nature and feasibility of the reaction with each adsorbent. The presence of various functional groups, such as the C=O group, C≡N, CH_3, CH_2, and CH, and the cavities on the surface facilitated the crystal violet adsorption. Overall, the experimental results revealed that

the efficiency of crystal violet adsorption increased up to 95% after the loading of copper oxide nanoparticles on the de-oiled *Glycine max* L. seeds. This work presents a low-cost, promising green adsorbent to smartly handle the removal of a toxic azo dye, *i.e.*, crystal violet.

Data availability

Data will be made available from the corresponding author upon reasonable request.

Author contributions

Mahnoor Usman: conceptualization, investigation, data curation, investigation, writing, formal analysis, visualization, and editing. Fozia Batool: conceptualization, visualization, methodology, resources, software, formal analysis, validation, supervision, project administration, funding acquisition, and writing – review & editing. Tunzeel Iqbal, Sobia Noreen, Humaira Yasmeen Gondal, Taleeha Roheen, Rahman Qadir, Muhammad Amin, Sayyam Sajid: conceptualization, visualization, methodology, resources, software, formal analysis, validation, and writing – review & editing. Allah Ditta: writing – review & editing, visualization, validation, software, resources, project administration, methodology, formal analysis, conceptualization. All the authors read and approved of the final manuscript.

Conflicts of interest

There are no conflicts to declare.

Acknowledgements

Notes and references

1 Z. M. Lazim, N. S. Zulkifli, T. Hadibarata and Z. Yusop, *J. Teknol.*, 2015, **74**(11), 147–151.
2 M. Saad, H. Tahir, J. Khan, U. Hameed and A. Saud, *Ultrason. Sonochem.*, 2017, **34**, 600–608.

3 Y. Chen, H. Xu, M. S. Khan, S. Han and S. Zhu, *Crit. Rev. Environ. Sci. Technol.*, 2025, **55**(14), 1097–1123.

4 S. Zhu, H. Xu, M. S. Khan, M. Xia, F. Wang and Y. Chen, *Water Res.*, 2025, **272**, 122997.

5 L. B. Shi, P. F. Tang, W. Zhang, Y. P. Zhao, L. C. Zhang and H. Zhang, *Trop. J. Pharmaceut. Res.*, 2017, **16**(1), 185–192.

6 D. Vaidehi, V. Bhuvaneshwari, D. Bharathi and B. P. Sheetal, *Mater. Res. Express*, 2018, **5**(8), 085403.

7 A. Rajendran, E. Siva, C. Dhanraj and S. Senthilkumar, *J. Bioprocess. Biotech.*, 2018, **8**(3), 324.

8 L. M. Guo, X. M. Xu, D. Zhao, X. G. Cai and B. Zhou, *AMB Express*, 2020, **10**, 1–13.

9 N. Sebeia, M. Jabli, A. Ghith and T. A. Saleh, *Arab. J. Chem.*, 2020, **13**(2), 4263–4274.

10 A. K. Singh and V. S. Raykar, *Colloid Polym. Sci.*, 2008, **286**, 1667–1673.

11 F. B. A. D. Freitas, M. Y. D. F. Câmara and M. D. F. Freire, *Blucher Chemistry Proceedings*, 2015, **3**(1), 610–618.

12 J. F. Honorio, M. T. Veit, G. D. C. Gonçalves, É. A. de Campos and M. R. Fagundes-Klen, *Water Sci. Technol.*, 2016, **73**(5), 1166–1174.

13 V. Srivastava and A. K. Choubey, *J. Mol. Struct.*, 2021, **1242**, 130749.

14 N. Gaur, A. Kukreja, M. Yadav and A. Tiwari, *Appl. Water Sci.*, 2018, **8**, 1–12.

15 J. M. Rami, C. D. Patel, C. M. Patel and M. V. Patel, *Mater. Today: Proc.*, 2021, **43**, 655–659.

16 M. A. Anderson and A. J. Rubin, *Soil Sci.*, 1982, **133**(4), 257–258.

17 W. F. Tan, S. J. Lu, F. Liu, X. H. Feng, J. Z. He and L. K. Koopal, *Soil Sci.*, 2008, **173**(4), 277–286.

18 M. B. Desta, *J. Thermodyn.*, 2013, **2013**(1), 375830.

19 I. A. W. Tan, A. L. Ahmad and B. H. Hameed, *Desalination*, 2008, **225**(1–3), 13–28.

20 J. Qin, F. Qiu, X. Rong, J. Yan, H. Zhao and D. Yang, *J. Appl. Polym. Sci.*, 2015, **132**(17), 41828.

21 Z. Yuan, J. Wang, Y. Wang, Q. Liu, Y. Zhong, Y. Wang, L. Li, S. F. Lincoln and X. Guo, *RSC Adv.*, 2019, **9**(37), 21075–21085.

22 F. Batool, S. Kanwal, H. Kanwal, S. Noreen, M. S. Hodhod, M. Mustaqeem, G. Sharif, H. K. Naeem, J. Zahid and A. R. Z. Gaafar, *Molecules*, 2023, **28**(20), 7124.

23 M. Sathiyabama, M. Indhumathi and T. Amutha, *Biocatal. Agric. Biotechnol.*, 2020, **29**, 101823.

24 T. Revathi and S. Thambidurai, *Int. J. Biol. Macromol.*, 2019, **139**, 867–878.

25 L. Jin, W. Li, Q. Xu and Q. Sun, *Cellulose*, 2015, **22**, 2443–2456.

26 Q. Li, Q. Yue, Y. Su and B. Gao, *Bioresour. Technol.*, 2011, **102**(9), 5290–5296.

27 P. Saha and S. Chowdhury, *Thermodynamics*, 2011, **16**, 349–364.

28 A. Adak, M. Bandyopadhyay and A. Pal, *Sep. Purif. Technol.*, 2005, **44**(2), 139–144.

29 J. S. Cao, J. X. Lin, F. Fang, M. T. Zhang and Z. R. Hu, *Bioresour. Technol.*, 2014, **163**, 199–205.

30 M. Ishaq, F. Javed, I. Amad, H. Ullah, F. Hadi and S. Sultan, *Iran. J. Chem. Chem. Eng.*, 2016, **35**(2), 97–106.

31 S. Li, *Bioresour. Technol.*, 2010, **101**(7), 2197–2202.

32 M. Alshabanat, G. Alsenani and R. Almufarij, *J. Chem.*, 2013, **2013**(1), 210239.

33 G. K. Cheruiyot, W. C. Wanyonyi, J. J. Kiplimo and E. N. Maina, *Sci. Afr.*, 2019, **5**, e00116.

34 M. Arami, N. Y. Limaee, N. M. Mahmoodi and N. S. Tabrizi, *J. Hazard. Mater.*, 2006, **135**(1–3), 171–179.

35 R. Gong, J. Sun, D. Zhang, K. Zhong and G. Zhu, *Bioresour. Technol.*, 2008, **99**(10), 4510–4514.

36 V. Chandane and V. K. Singh, *Desalination Water Treat.*, 2016, **57**(9), 4122–4134.

37 A. R. Bagheri, M. Ghaedi, A. Asfaram, S. Hajati, A. M. Ghaedi, A. Bazrafshan and M. R. Rahimi, *J. Taiwan Inst. Chem. Eng.*, 2016, **65**, 212–224.

38 S. D. Abkenar, M. R. Ganjali, M. Hosseini and M. S. Karimi, *Iran. J. Chem. Chem. Eng.*, 2019, **38**(6), 83–92.

39 T. B. Vidovix, H. B. Quesada, R. Bergamasco, M. F. Vieira and A. M. S. Vieira, *Environ. Technol.*, 2022, **43**(20), 3047–3063.

40 S. K. Shukla, S. Pandey, S. Saha, H. R. Singh, P. K. Mishra, S. Kumar and S. K. Jha, *J. Environ. Chem. Eng.*, 2021, **9**(5), 105847.

41 S. K. Das, M. M. R. Khan, T. Parandhaman, F. Laffir, A. K. Guha, G. Sekaran and A. B. Mandal, *Nanoscale*, 2013, **5**(12), 5549–5560.

42 R. K. Devi, G. Venkateswarlu, P. R. Kumar, Y. Nagaiah, S. K. Akmal and Y. Vijaya, *Int. J. Res. Anal. Rev.*, 2018, **5**, 483–491.

43 A. Ghaffar, S. Kiran, M. A. Rafique, S. Iqbal, S. Nosheen, Y. Hou, G. Afzal, M. Bashir and U. Aimun, *Desalination Water Treat.*, 2021, **212**, 368–375.

44 S. Y. S. Zeebaree, A. Y. S. Zeebaree, O. I. H. Zebari and A. Y. S. Zebari, *Curr. Res. Green Sustainable Chem.*, 2021, **4**, 100103.